Applied Thermal Engineering 220 (2023) 119710

Contents lists available at ScienceDirect

Applied Thermal Engineering

journal homepage: www.elsevier.com/locate/apthermeng

Research Paper

Seasonal energy efficiency ratio of regenerative indirect evaporative coolers—Simplified calculation method

María Jesús Romero-Lara [a,*], Francisco Comino [b], Manuel Ruiz de Adana [a]

[a] Departamento de Química-Física y Termodinámica Aplicada, Escuela Politécnica Superior, Universidad de Córdoba, Campus de Rabanales, Antigua Carretera Nacional IV, km 396, 14071 Córdoba, Spain
[b] Departamento de Mecánica, Escuela Politécnica Superior, Universidad de Córdoba, Campus de Rabanales, Antigua Carretera Nacional IV, km 396, 14071 Córdoba, Spain

ARTICLE INFO

Keywords:
Coefficient of performance
Energy efficiency
Experimental tests
Indirect evaporative cooling
Seasonal Energy Efficiency Ratio

ABSTRACT

Evaporative-cooling technology is a promising alternative to conventional air-cooling systems that are based on using direct expansion units in terms of energy efficiency. Seasonal energy efficiency ratio (SEER) calculation methodologies and standards for these air-cooling systems remain limited. Therefore, the objective of this study is to develop a novel simplified method for calculating the SEER for regenerative indirect evaporative coolers (RIEC). Experimental tests were performed to obtain energy efficiency ratio models of four RIEC systems. Five climate zones in the Mediterranean region were considered for calculation of the SEER values. A detailed calculation method based on annual energy simulations was employed, and the results of the seasonal index were compared with those of a simplified calculation method based on the steady-state operation at four specific test points. The relative error between the SEER calculation methods was 4.6% for all the RIEC systems and climate zones. The highest SEER values of 5.8 and 5.5 were achieved for the Cairo and Madrid weather conditions, respectively. This study can serve as a reference for research on the seasonal performance and life-cycle analysis of RIEC based on an efficient counterflow heat exchanger with a wide range of airflow and cooling capacities.

1. Introduction

Evaporative-cooling technology is a potential alternative to conventional heating, ventilation, and air conditioning (HVAC) systems in terms of energy savings. There are two main types of evaporative coolers—direct evaporative coolers (DEC) and indirect evaporative coolers (IEC). In DEC systems, the inlet airflow and 100% outdoor air are in direct contact with water. Water evaporation and air temperature reduction occurs simultaneously with the addition of moisture to the supply air of the DEC system. In IEC systems, the inlet airflow and water are separated by alternating wet and dry channels, while maintaining a constant inlet humidity ratio [1]. IEC systems have also been combined with other technologies, such as desiccant systems [2,3], to obtain high energy performance.

Previous studies have examined the influence of the IEC design and configuration on energy performance, as well as the different types of IEC configurations. They include traditional IEC [4], dew-point indirect evaporative coolers (DIEC) [5,6], Maisotsenko cycle-based indirect evaporative coolers (MIEC) [7,8], and regenerative indirect evaporative coolers (RIEC) [9,10]. IEC systems are classified as plate-type crossflows [11], plate-type counterflows [12], tube types [13], and heat pipes [14]. The counterflow arrangement has been found to be more energy-efficient than the crossflow arrangement [15]. The optimal operational parameters and geometric design of the DIEC according to the European ventilation regulations were determined in another study [16], wherein the maximum EER values were obtained at low volumetric airflow rates. These high EER values were approximately 37.1 and 50.2 for the auditorium and office applications, respectively. Table 1 summarises each indirect evaporative cooling technology (IEC, DIEC, MIEC, and RIEC) as well as the working conditions and the corresponding EER values.

Different plastic materials, such as polyethylene terephthalate (PET) and PET/cellulose composite materials, have been used in the construction of IEC systems [21]. It should be noted that several studies have developed the application of porous materials for IEC of plate-type geometry [22–24]. These studies reported that low evaporation, owing to poor wettability of the channel wet surface, significantly reduced the cooling performance.

Several studies have focused on the difference in EER values between

* Corresponding author.
E-mail address: p42rolam@uco.es (M.J. Romero-Lara).

https://doi.org/10.1016/j.applthermaleng.2022.119710
Received 15 July 2022; Received in revised form 17 October 2022; Accepted 20 November 2022
Available online 25 November 2022

Nomenclature

b	estimated parameter
CDD	cooling degree-days
DIEC	dew-point indirect evaporative cooler
DOE	design of experiments
DX	direct expansion unit
EER	Energy efficiency ratio [-]
f	fan
h	air specific enthalpy [kJ·kg^{-1}]
H	hours
HDD	heating degree-days
HVAC	heating, ventilation, and air conditioning
IEC	indirect evaporative cooler
MAE	mean absolute error
MIEC	Maisotsenko cycle-based indirect evaporative cooler
p	pump
P	pressure drop [Pa]
PLF	partial load factor [-]
Q	thermal energy [kWh]
$\dot{Q}$	thermal power [kW]
R	rate [-]
R^2	coefficient of determination [-]
RE	relative error [%]
RH	relative humidity [%]
RIEC	regenerative indirect evaporative cooler
SEER	seasonal energy efficiency ratio [-]
T	temperature [°C]
TRNSYS	transient system simulation
$\dot{V}$	volumetric airflow rate [m^3·h^{-1}]
W	energy consumption [kWh]
$\dot{W}$	power consumption [kW]
X	input variable
$\hat{Y}$	estimated output value

Greek letters

$\sum$	sum
ρ	density [kg·m^{-3}]
ω	humidity ratio [g·kg^{-1}]

Subscripts

A	Experimental test point A
avg	average
B	Experimental test point B
C	Experimental test point C
D	Experimental test point D
EA	exhaust air
nom	nominal
OA	outdoor air
SA	supply air
wb	wet bulb

Table 1
Summary of IEC technologies and EER values.

IEC configuration	Working conditions	EER [-]	Reference
IEC	Inlet temperature = 24–35 °C Inlet relative humidity = 35–65% Volumetric flow rates = 600–1050 m^3·h^{-1}	6–16 (Experimental model)	[17]
DIEC	Inlet temperature = 25–45 °C Inlet relative humidity = 12.5–50% Air velocity = 0.3–3.3 m·s^{-1}	Up to 60 (Statistical model)	[18]
MIEC	Inlet temperature = 25–40 °C Inlet relative humidity = 30–70% Mass flow rates = 0.1–0.26 kg·s^{-1}	Up to 130 (Mathematical model)	[19]
RIEC	Inlet temperature = 22.7–38.9 °C Inlet humidity ratio = 9.3–19.4 g·kg^{-1} Air velocity = 1.58–2.83 m·s^{-1}	2.8–15.5 (Experimental model)	[20]

IEC and traditional HVAC systems, and the influence of outdoor-air conditions. One study demonstrated that IEC technology for air handling units (AHU) improved the EER by 67% compared to that without IEC. In an IEC system, the EER value increased from 4.3 to 7.2 [25]. An assessment of an MIEC in terms of the coefficient of performance revealed that the EER value improved by 26% compared to conventional air-cooling systems [26]. In this novel system, an exhaust-air heat pump with an IEC recovery and four modes of operation was used for model validation [27]. The results of these tests showed that the EER value increased by 135% compared to that of traditional exhaust-air heat pumps. According to the outdoor-air conditions, other experimental tests in an RIEC showed that the EER value varied between 10.6 and 19.7. The lowest EER value (10.6) was obtained for high values of the outdoor-air humidity ratio and low values of outdoor-air temperature. By contrast, the highest EER value (19.7) was obtained for a low outdoor air humidity ratio and high outdoor air temperature [28]. Another study on the energy behaviour of an MIEC under different working conditions was conducted [29], wherein the maximum EER value of approximately 19 was obtained for high outdoor air temperature values (43–45 °C) and low outdoor air humidity values (approximately 10 g·kg^{-1}). A recent study concluded that the EER of a DIEC significantly reduces when outdoor-air humidity increases. Therefore, the DIEC system exhibits higher energy performance values in hot arid areas [30]. This study also reported that a newly patented DIEC, with parallel ducts for handling product air and energy recovery modes, could be applied to hot and medium-to-high humidity climate zones.

Variations in inlet air temperature and humidity influence the energy performance of cooling systems. Therefore, the EER value at a particular point does not indicate the seasonal performance of a cooling system. Several studies have employed mathematical models in conjunction with energy-simulation tools to compare the annual energy performance of different air-cooling systems. In one such study, an RIEC system exhibited energy consumption values three to four times lower than those of a conventional air-cooling system for the same energy demand in the severe climates of Lampedusa and Seville [31]. Other studies have calculated the seasonal energy efficiency ratio (SEER) value in evaporative coolers during summer periods; for example, from 1 June to 31 August [32–34]. The main finding of these studies was that the use of IEC technology increased the SEER by 35–50% compared to conventional HVAC systems. Annual energy simulations or experimental data are necessary to obtain SEER values in IEC systems, because standard regulations pertaining to these values have not been developed. The Eurovent Certita Certification specifies the test point positions to obtain the wet bulb effectiveness value in IEC systems [35], but it does not

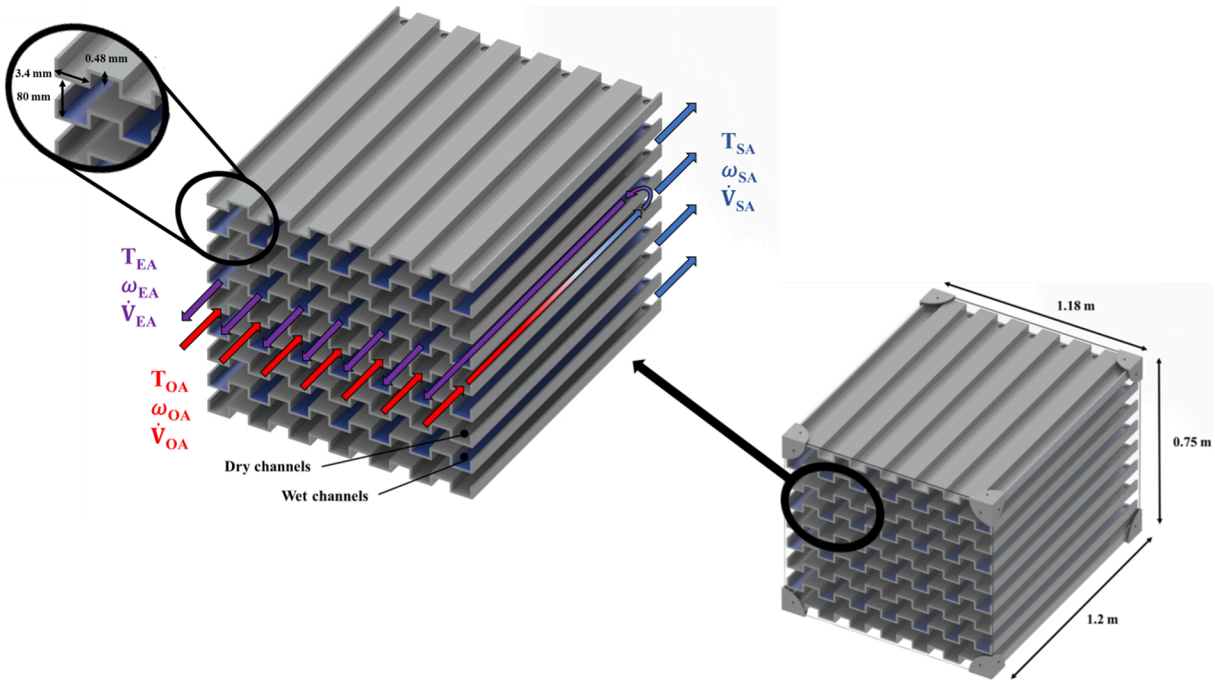

Fig. 1. Schematic of the heat exchanger in the RIEC system.

provide a methodology for calculating the SEER value in IEC. Other standards and regulations specify the test points and SEER calculation method for heat pumps and chillers [36,37]. Several studies have performed seasonal energy analyses of heat pumps [38–40]. However, most studies on IEC technologies have focused on the instantaneous performance [41,42]. Another study developed a 'seasonal utilizability factor', but an energy simulation was necessary to complete this study [43]. Currently, a seasonal performance value/SEER is required for the IEC to calculate renewable cooling energy according to the recent Delegated Regulation (EU) 2022/759 of the Commission document [44].

To address the research gap regarding seasonal energy performance indices for evaporative-cooling systems without the need for energy simulations or annual experimental data, this study developed a novel simplified method for calculating the SEER for RIEC. To achieve this objective, several experimental tests were performed to obtain empirical RIEC models for the EER in European climates. The proposed SEER calculation method was then compared with the traditional method.

2. Methodology

2.1. Constructive and operational characteristics of RIEC systems

Four regenerative IECs, RIEC-1, RIEC-2, RIEC-3, and RIEC-4 were experimentally analysed in this study. The RIEC systems were mainly composed of a counterflow heat exchanger, process fan, *coarse 60%* category filter located between the process fan and the heat exchanger, and fine filter (ePM_1 *65%*) according to the European Standard EN 16890–1 [45], on the supply air side. The working principle of heat exchangers is that a single inlet air stream where 100% outdoor air (OA) enters each RIEC system and is divided into two air streams: exhaust air (EA) and supply air (SA). This nomenclature was adopted in accordance with the European Standard EN 16798–3 [46]. All the heat exchangers consisted of alternating wet and dry channels separated by thin plates. OA circulated through the dry channels and exchanged heat with the wet channels. The primary OA stream was cooled with no added moisture and was supplied to the building. In the secondary air stream, a fraction of the OA entered the wet channels and was humidified by water evaporation, whereafter it exhausted outside as EA. The relationship between the EA and OA flow is defined by the exhaust-air rate (REA) as shown in Eq. (1).

$$REA = \frac{\dot{V}_{EA}}{\dot{V}_{OA}} \quad (1)$$

Table 2
Main characteristics of the selected RIEC systems.

RIEC nomenclature	$\dot{V}_{SA,nom}$ [$m^3 \cdot h^{-1}$]	$\dot{Q}_{cooling,nom}$ [kW]	$\dot{W}_{nom}$ [kW]	Dimensions (Long × Wide × High) [m]	Cores [-]
RIEC-1	2880	18	1.5	2.33 × 1.23 × 1.61	2
RIEC-2	3960	24	1.8	2.33 × 1.83 × 1.29	3
RIEC-3	23,040	59	10	4.47 × 2.31 × 2.55	16
RIEC-4*	46,080	118	20	6.00 × 4.62 × 5.10	32

* The RIEC-4 system is equivalent to a set of two RIEC-3 systems in parallel.

Based on the constructive characteristics of these RIEC systems, the walls of the heat exchanger were composed of PVC film with a hydrophilic material. The main geometrical features of the common heat exchangers in the four RIEC systems are shown in Fig. 1.

The RIEC systems considered in this study have the same working principles and are commercially available. However, these RIEC systems have different numbers of heat-exchange cores arranged in parallel. Thus, the four RIEC systems had different nominal airflow rates, cooling capacities, input powers, and dimensions (see Table 2).

2.2. Experimental setup

An experimental facility was built to analyse the RIEC-1 performance under different working conditions (see Fig. 2). The OA temperature, outdoor-air humidity ratio, and outdoor volumetric airflow in each experimental test were adjusted using an AHU. The exhaust-air rate (R_{EA}) was adjusted for each experimental test, according to Eq. (1).

Several sensors for air temperature (T) and relative humidity (RH) for each air stream (OA, EA, and SA), pressure drop (P) at the outlet of RIEC-1, volumetric air flow ($\dot{V}$), and electrical power consumption ($\dot{W}$) were used to register the RIEC-1 working conditions. The locations of the

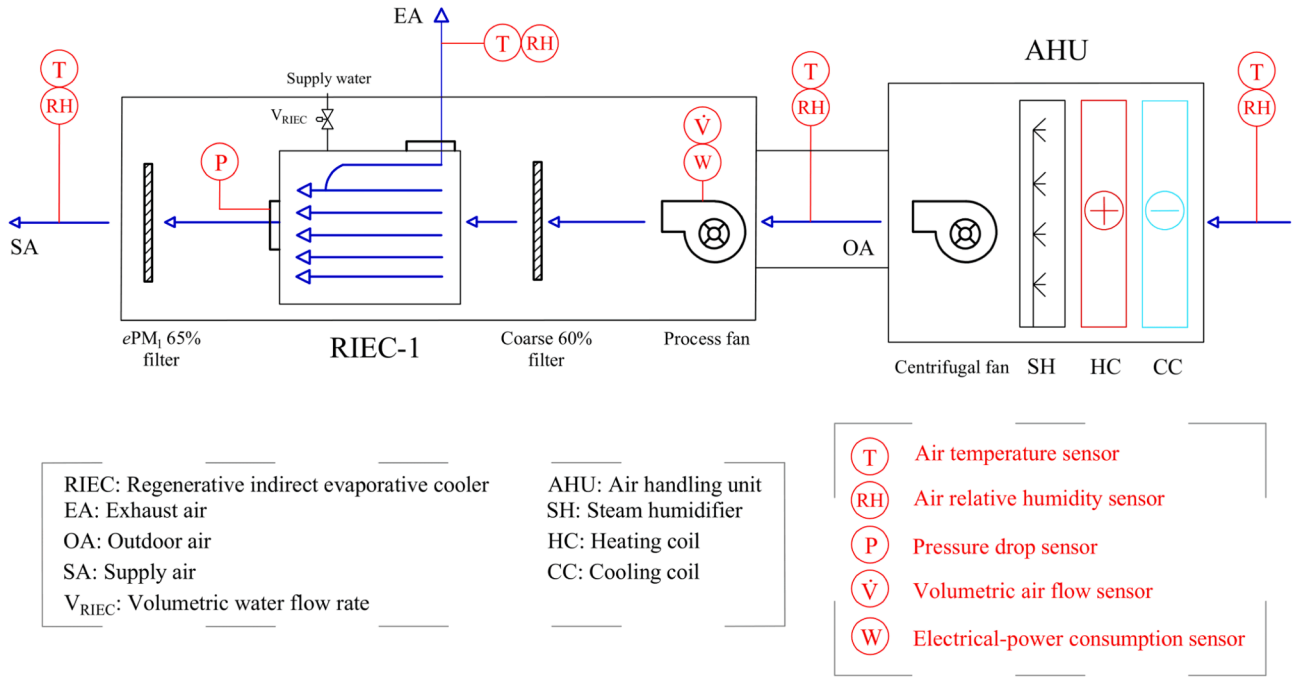

Fig. 2. Schematic of the experimental setup.

Table 3
Types and accuracies of sensors used in the experimental setup.

Variable	Type of sensor	Accuracy
T	PT100	±0.2 °C (range of 0 to 50 °C)
RH	Capacitive	±3% (range of 0 to 90%)
P	Piezo-resistive	±0.05 hPa (range of −150 to 150 hPa)
V̇	Differential pressure transmitter	±5% (range < 500 Pa)
Ẇ	3-phase	±1% measurement (range of 0.01 to 9.99 kW)

Table 4
Input variables for the design of experiments for the four RIEC systems.

Input variable	Values	Unit
Outdoor-air temperature, T_{OA}	29.0–35.5–43.0	°C
Outdoor-air humidity ratio, ω_{OA}	8.9–10.9–12.6	$g{\cdot}kg^{-1}$
Exhaust-air rate, R_{EA}	0.3–0.5–0.7	–
Outdoor volumetric air flow, $\dot{V}_{OA}$	3019–3692–4587	$m^3{\cdot}h^{-1}$

sensors in the experimental facility are illustrated in Fig. 2. The types and accuracies of these sensors are listed in Table 3.

2.3. Experimental tests conditions

Experimental tests under different working conditions were performed to develop empirical models of the four RIEC systems to obtain the cooling capacity, $\dot{Q}_{cooling}$, electrical power consumption, $\dot{W}$, and energy efficiency ratio (EER) for each experimental test, performed for a steady-state period of 30 min. The experimental tests were based on the statistical technique of the 'design of experiments'; specifically, the Box–Behnken design. The design consists of 27 experimental tests with three central points. The input parameters of the experimental tests were the outdoor air temperature (T_{OA}), outdoor air humidity ratio (ω_{OA}), outdoor volumetric airflow ($\dot{V}_{OA}$), and R_{EA}. The ranges of the input parameter values are listed in Table 4.

A summary of the OA conditions and value of the R_{EA} for each experimental test is shown in Table 5.

The experimental tests were performed in RIEC-1 by the authors, while the RIEC-2, RIEC-3, and RIEC-4 experimental tests were performed by the manufacturer [47].

2.4. Empirical RIEC models

The energy behaviour of the RIEC system was analysed using the following instantaneous performance indices: cooling capacity ($\dot{Q}_{cooling}$), electrical power consumption ($\dot{W}$), and EER. The performance of the four RIEC systems was evaluated by analysing the results of 27 experimental tests, as indicated in Table 5.

The cooling capacities of the RIEC systems in each experimental test were calculated using Eq. (2):

$$\dot{Q}_{cooling} = \rho_{air}\hat{A}{\cdot}_{SA}\hat{A}{\cdot}(h_{OA} - h_{SA}) \quad (2)$$

where ρ_{air} is the air density [$kg{\cdot}m^{-3}$], $\dot{V}_{SA}$ is the supply volumetric airflow [$m^3{\cdot}s^{-1}$], h_{OA} is the OA specific enthalpy [$kJ{\cdot}kg^{-1}$], and h_{SA} is the supply air specific enthalpy [$kJ{\cdot}kg^{-1}$].

The electrical power consumed in each RIEC system ($\dot{W}$) was calculated for each experimental test. It was obtained by considering the sum of the electrical power consumed by the process fan ($\dot{W}f$) and that consumed by the pump ($\dot{W}p$), as shown in Eq. (3).

$$\dot{W} = \dot{W}f + \dot{W}p \quad (3)$$

The EER was calculated for each experimental test using Eq. (4).

$$EER = \frac{\dot{Q}_{cooling}}{\dot{W}} \quad (4)$$

Second-order polynomial equations were used to obtain the relationship between the input parameters and instantaneous performance indices, as shown in Eq. (5), where $\hat{Y}$ is the instantaneous performance index ($\dot{Q}_{cooling}$, $\dot{W}$, and EER); X represents the input parameters (T_{OA}, ω_{OA}, $\dot{V}_{OA}$, and R_{EA}); b_0 is the average response in each model; and b_i, b_{ii}, and b_{ij} are the estimated parameters of the linear, quadratic, and second-order terms, respectively.

Table 5
Summary of experimental test conditions for empirical RIECs models.

Test	T_{OA}	ω_{OA}	$\dot{V}_{OA}$	R_{EA}	Test	T_{OA}	ω_{OA}	$\dot{V}_{OA}$	R_{EA}
	[°C]	[g·kg^{-1}]	[m^3·h^{-1}]	[-]		[°C]	[g·kg^{-1}]	[m^3·h^{-1}]	[-]
N1	29.0	8.9	3692	0.5	N15	29.0	10.9	4587	0.5
N2	35.5	8.9	3692	0.7	N16	29.0	10.9	3019	0.5
N3	35.5	8.9	3692	0.3	N17	29.0	10.9	3692	0.3
N4	43.0	8.9	3692	0.5	N18	29.0	10.9	3692	0.7
N5	35.5	8.9	4587	0.5	N19	29.0	12.6	3692	0.5
N6	35.5	8.9	3019	0.5	N20	35.5	12.6	3692	0.3
N7	43.0	10.9	4587	0.5	N21	35.5	12.6	3692	0.7
N8	43.0	10.9	3692	0.7	N22	43.0	12.6	3692	0.5
N9	43.0	10.9	3692	0.3	N23	35.5	12.6	3019	0.5
N10	43.0	10.9	3019	0.5	N24	35.5	12.6	4587	0.5
N11	35.5	10.9	3019	0.3	N25	35.5	10.9	3692	0.5
N12	35.5	10.9	3019	0.7	N26	35.5	10.9	3692	0.5
N13	35.5	10.9	4587	0.7	N27	35.5	10.9	3692	0.5
N14	35.5	10.9	4587	0.3					

[a] Tests N25, N26, and N27 were central points of the design of experiments.

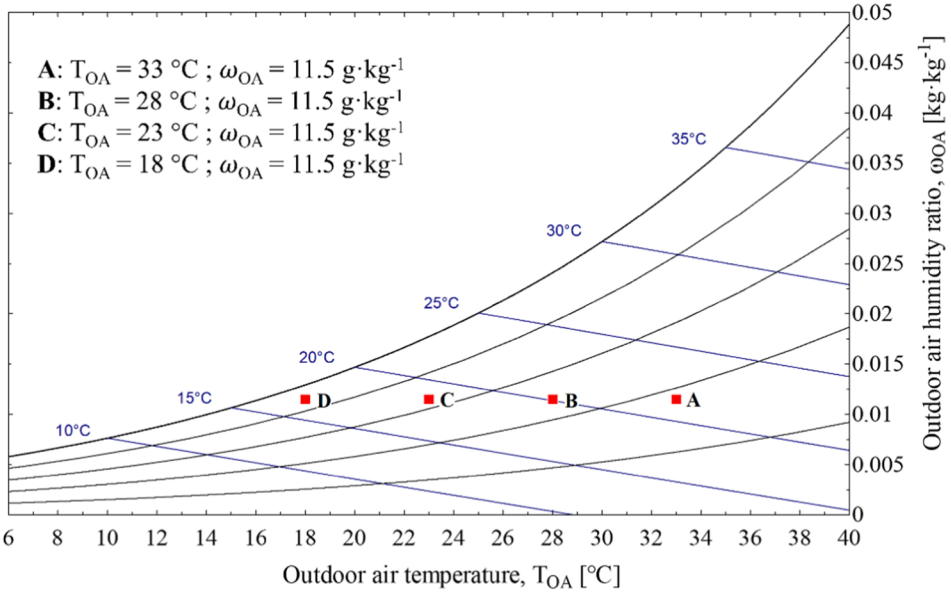

Fig. 3. Specific OA conditions at the four experimental test points.

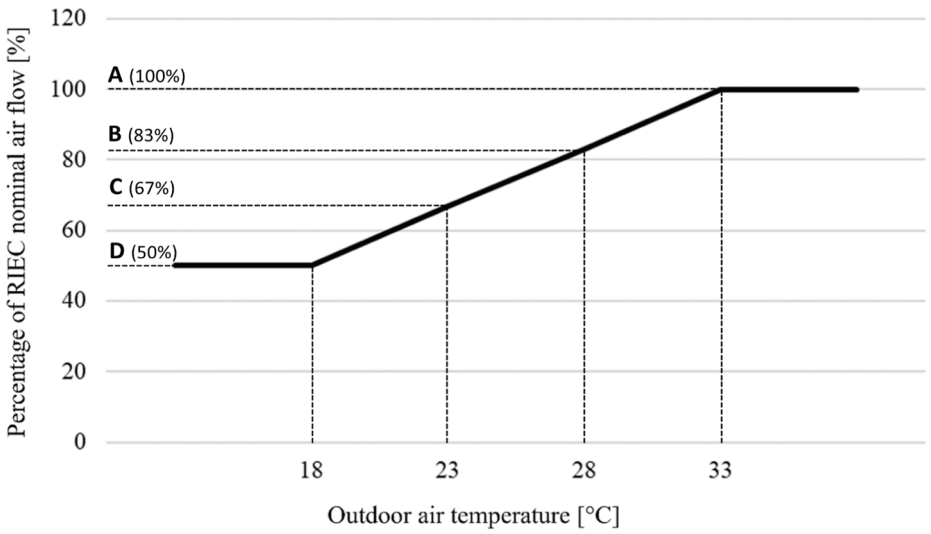

Fig. 4. Cooling capacity control strategy for the four RIEC systems.

Table 6
Summary of experimental test conditions and *PLF* for the simplified SEER method.

Test	T_{OA}	ω_{OA}	$\dot{V}_{SA,nom}$	*PLF*
	[°C]	[g·kg^{-1}]	[%]	[-]
A	33	11.5	100	1.00
B	28	11.5	83	0.83
C	23	11.5	67	0.67
D	18	11.5	50	0.50

$$\hat{Y} = b_0 + \sum_{i=1}^{k} b_i \cdot X_i + \sum_{i=1}^{k} b_{ii} \cdot X_i^2 + \sum_{i=1}^{k=1} \sum_{i=2j>i}^{k} b_{ij} \hat{A} \cdot X_i \hat{A} \cdot X_j \quad (5)$$

2.5. Seasonal energy efficiency ratio (SEER)

The SEER expresses the seasonal behaviour of the RIEC system in terms of energy performance. This seasonal index was calculated for the cooling period, which was defined as the number of hours during which the outdoor air temperature exceeded 18 °C. Two different calculation methods were established to obtain the SEER value in the RIEC systems: (i) a simplified SEER calculation method and (ii) a detailed SEER calculation method.

2.5.1. Simplified SEER calculation method

This simplified method of testing and calculating the SEER in RIEC systems consisted of conducting four experimental tests (A, B, C, and D) under specific OA conditions, following an approach similar to that described in the European Standard EN 14825:2018 [36] for 'other' HVAC systems. Different OA temperatures and supply volumetric airflows were considered to obtain the values of $\dot{Q}_{cooling}$, $\dot{W}$, and *EER* in Tests A, B, C, and D. The value of the outdoor-air humidity ratio was constant for the four experimental tests (11.5 g·kg^{-1}). This humidity was the average value calculated for the five climate zones selected from the Mediterranean climate region. The maximum T_{OA} value for the five selected climate zones in the Mediterranean climate region was 33 °C. Therefore, the range of T_{OA} values for the four experimental tests was 18–33 °C, with a difference of 5 °C between the experimental tests. The four experimental tests performed using the simplified method to obtain the SEER values is shown in Fig. 3.

Controlling the cooling capacity by temperature manipulation was established in the RIEC system. The control was based on four different percentages of the RIEC nominal airflow obtained according to the OA temperature, as shown in Fig. 4. This control strategy was based on the European Standard EN 14825:2018 for the calculation of SEER in air conditioners, chillers, and heat pumps [36]. For each test (A, B, C, and D), a partial load factor (PLF) was used to calculate the SEER value using the simplified method. The PLF values were established from 0 to 1, with a determined range for each PLF according to the European Standard [36]. However, these ranges must be adjusted to minimise the SEER calculation error between the proposed and traditional methodologies based on energy simulations. These PLF values were constant for the four RIEC systems and five climate zones (see Table 6).

The airflow rate of the RIEC system was adjusted from 50 to 100% of the nominal volumetric airflow, according to the OA temperature in the range of 18–33 °C, as shown in Fig. 4.

The RIEC systems worked at 100% of their nominal airflow for T_{OA} equal to 33 °C in partial load test A, 83% of their nominal airflow for T_{OA} equal to 28 °C in partial load test B, 67% of their nominal airflow for T_{OA} equal to 23 °C in partial load test C, and 50% of their nominal airflow for T_{OA} equal to 18 °C in partial load test D. If the T_{OA} value was below 18 °C, no cooling-energy demand was considered; however, the fan continued to operate at 50%, as shown in Fig. 4.

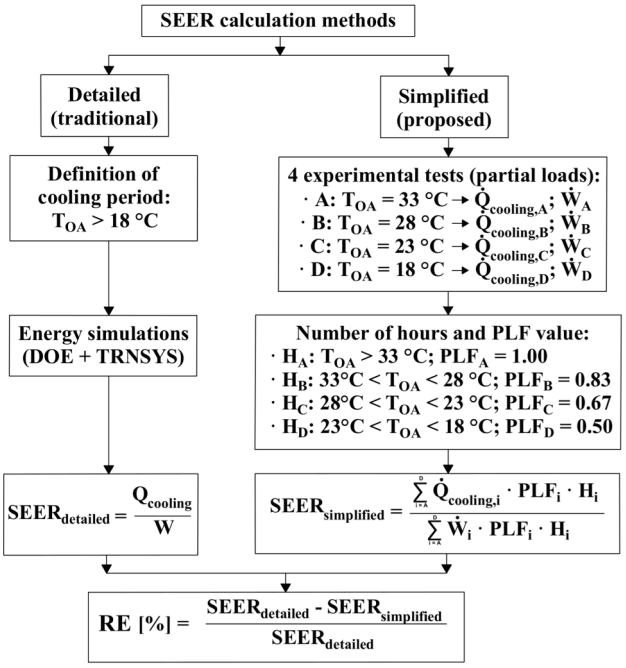

Fig. 5. Scheme of methodologies for calculating the SEER value in RIEC.

The number of hours at each partial load (A, B, C, and D) was calculated for different ranges of OA temperatures for each Mediterranean climate zone. The number of hours of RIEC work at partial loads A (H_A), B (H_B), C (H_C), and D (H_D) was the sum of the hours when T_{OA} exceeded 33 °C, or was between 28 and 33 °C, 23–28 °C, and 18–23 °C, respectively. The simplified SEER value was calculated using Eq. (6).

$$SEER_{simplified} = \frac{\dot{Q}_{cooling,A} \hat{A} \cdot PLF_A \hat{A} \cdot H_A + \dot{Q}_{cooling,B} \hat{A} \cdot PLF_B \hat{A} \cdot H_B + \dot{Q}_{cooling,C} \hat{A} \cdot PLF_C \hat{A} \cdot H_C + \dot{Q}_{cooling,D} \hat{A} \cdot PLF_D \hat{A} \cdot H_D}{\dot{W}_A \hat{A} \cdot PLF_A \hat{A} \cdot H_A + \dot{W}_B \hat{A} \cdot PLF_B \hat{A} \cdot H_B + \dot{W}_C \hat{A} \cdot PLF_C \hat{A} \cdot H_C + \dot{W}_D \hat{A} \cdot PLF_D \hat{A} \cdot H_D} \quad (6)$$

Here, for each RIEC, $\dot{Q}_{cooling}$ and $\dot{W}$ are the integrated energy-cooling capacity and integrated electrical power consumption, respectively, for the four OA conditions tested (see Table 6). The number of hours for each partial load (H) was a characteristic value for each climate zone. The H_A, H_B, H_C, and H_D results for each Mediterranean climate zone were obtained using the 'meteonorm' data [48].

2.5.2. Detailed SEER calculation method

The total cooling capacity and energy consumption during a seasonal period can be calculated by collecting long-term data or by using energy-simulation tools. In this study, seasonal energy simulations were performed using the empirical models of $\dot{Q}_{cooling}$, $\dot{W}$, and *EER* to obtain detailed SEER values. Annual energy simulations were performed using the TRNSYS17 software [49], with a time step of 2.4 min. The weather conditions were generated using 'meteonorm' data. For the detailed method, the SEER values were calculated using Eq. (7):

$$SEER_{detailed} = \frac{\sum \dot{Q}_{cooling}}{\sum \dot{W}} = \frac{Q_{cooling}}{W} \quad (7)$$

Table 7
Selected climatic zones in the Mediterranean region.

City (Country)	Köppen–Geiger	Climate definition	$T_{OA,avg}$ [°C]	$\omega_{OA,avg}$ [g·kg^{-1}]	Cooling period [h]	CDD[a] and HDD[b]
Cairo (Egypt)	BWh	B: arid W: desert h: hot arid	25.0	10.0	5850.2	3500 < CDD ≤ 5000
Murcia (Spain)	BSk	B: arid S: steppe k: cold arid	22.6	10.1	3817.2	CDD < 3500 HDD ≤ 2000
Pescara (Italy)	Cfb	C: warm temperate f: fully humid b: warm summer	22.9	11.6	2955.0	CDD < 3500 HDD ≤ 2000
Napoli (Italy)	Csa	C: warm temperate s: summer dry a: hot summer	23.1	12.1	3441.0	CDD < 3500 HDD ≤ 2000
Madrid (Spain)	Csb	C: warm temperate s: summer dry b: warm summer	24.0	9.9	2740.0	CDD < 3500 2000 < HDD ≤3000

[a] T_{base} = 10 °C for cooling degree-days; [b] T_{base} = 18 °C for heating degree-days.

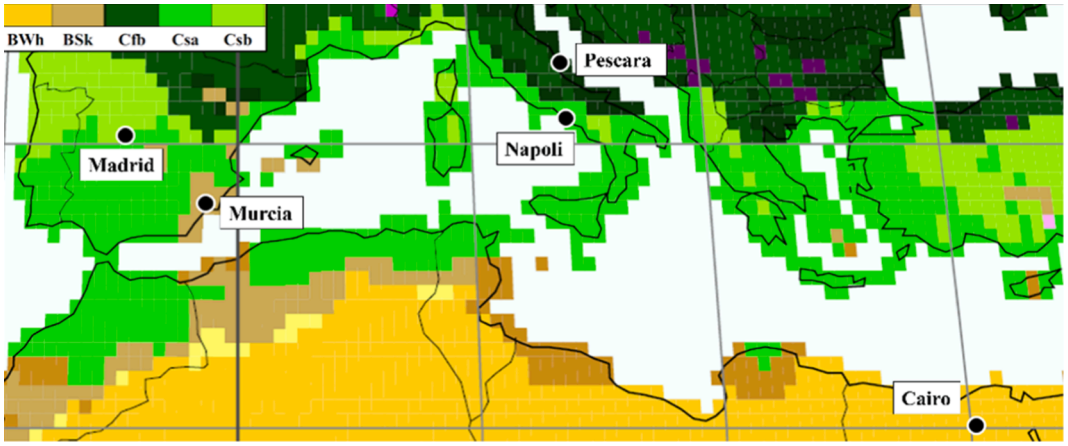

Fig. 6. Map of the Mediterranean region according to the Köppen–Geiger climate classification.

where $Q_{cooling}$ and W represent the annual cooling energy and energy consumption of the RIEC system, respectively. The cooling capacity control strategy is similar to that used in the simplified method, as shown in Fig. 4. The results of both the SEER calculation methods were compared with the relative error (RE), as shown in Eq. (8). A summary scheme of both the SEER calculation methods is shown in Fig. 5.

$$RE = \frac{SEER_{detailed} - SEER_{simplified}}{SEER_{detailed}} \quad (8)$$

2.6. Climate zones of Mediterranean region

The SEER values, $SEER_{detailed}$, and $SEER_{simplified}$ for the four RIEC systems were calculated and analysed for the five climate zones in the Mediterranean region. The Köppen–Geiger climate classification method was used to select cities that represented these climate zone [50]. The mean values of the outdoor-air temperature ($T_{OA,avg}$) and outdoor-air humidity ratio ($\omega_{OA,avg}$) during the respective cooling periods are listed in Table 7. The cooling degree-days, CDD, heating degree-days, HDD, and number of hours during the cooling period for each city are also listed in Table 7. It can be observed that typical Mediterranean climate zones include cities with cold arid to hot summer climates, according to the corresponding variation in average $T_{OA,avg}$ and $\omega_{OA,avg}$ of each climate zone. A map of these climate zones in the Mediterranean region is shown in Fig. 6.

3. Results and analysis

In this study, the EER and SEER were analysed for the four RIEC systems. Several empirical RIEC models have been used to develop both parameters. SEER values were obtained using two simplified and detailed calculation methods, as shown in Fig. 5.

3.1. Experimental results of EER

A set of experimental tests were carried out for the RIEC-1 system to obtain values of $\dot{Q}_{cooling}$, $\dot{W}$, and EER under different working conditions (N1–N27), as shown in Table 5 and the results of these indices were obtained using Eqs. (2), (3), and (4), respectively. The values of these output parameters and the uncertainty for each experimental test are summarised in Table 8. The uncertainty was calculated according to the 'Guide to the Expression of Uncertainty in Measurement' (GUM) [51]. The range of the results of $\dot{Q}_{cooling}$, $\dot{W}$, and EER were from 4.0 to 17.2 kW, 0.4 to 1.2 kW and 6.0 to 26.6 kW, respectively. The minimum EER value of 6.0 was obtained for test N18, with the minimum value of T_{OA} (29.0 °C), and the maximum value of R_{EA} (0.7). The minimum $\dot{Q}_{cooling}$ value was obtained for this test. The maximum EER value was achieved under the operating conditions of test N10 (26.6), with a maximum T_{OA} value of 43 °C and a minimum $\dot{V}_{OA}$ value of 3019 m^3·h^{-1}. The lowest and highest $\dot{W}$ values of 0.4 kW and 1.2 kW, respectively, were achieved when RIEC-1 was operating with inlet air flow rates of 3019 and 4587 m^{-3}·h^{-1}, respectively.

Table 8
Experimental results of the RIEC-1 system.

Test	$\dot{Q}_{cooling}$	$\dot{W}$	*EER*	Test	$\dot{Q}_{cooling}$	$\dot{W}$	*EER*
	[kW]	[kW]	[-]		[kW]	[kW]	[-]
N1	8.4 ± 0.7	0.7 ± 0.007	12.0 ± 0.9	N15	7.7 ± 0.8	1.2 ± 0.012	6.5 ± 0.7
N2	7.5 ± 0.4	0.7 ± 0.007	11.3 ± 0.6	N16	5.3 ± 0.5	0.4 ± 0.004	13.1 ± 1.3
N3	14.2 ± 0.9	0.7 ± 0.007	20.7 ± 1.3	N17	8.7 ± 0.9	0.7 ± 0.007	12.7 ± 1.3
N4	15.0 ± 0.7	0.7 ± 0.007	21.4 ± 1.0	N18	4.0 ± 0.4	0.7 ± 0.007	6.0 ± 0.6
N5	14.2 ± 0.8	1.2 ± 0.012	12.0 ± 0.7	N19	4.4 ± 0.7	0.7 ± 0.007	6.2 ± 0.9
N6	9.1 ± 0.5	0.4 ± 0.004	22.4 ± 1.4	N20	10.4 ± 0.9	0.7 ± 0.007	15.1 ± 1.4
N7	16.0 ± 0.8	1.2 ± 0.012	13.5 ± 0.7	N21	4.4 ± 0.4	0.7 ± 0.007	6.6 ± 0.6
N8	8.4 ± 0.4	0.7 ± 0.007	12.6 ± 0.6	N22	11.2 ± 0.7	0.7 ± 0.007	15.9 ± 1.0
N9	17.2 ± 0.9	0.7 ± 0.007	25.1 ± 1.4	N23	6.2 ± 0.5	0.4 ± 0.004	15.3 ± 1.4
N10	10.8 ± 0.6	0.4 ± 0.004	26.6 ± 1.4	N24	8.5 ± 0.8	1.2 ± 0.012	7.1 ± 0.7
N11	10.2 ± 0.8	0.4 ± 0.004	25.5 ± 1.9	N25	10.4 ± 0.7	0.7 ± 0.007	14.8 ± 0.9
N12	4.9 ± 0.3	0.4 ± 0.004	12.3 ± 0.9	N26	10.4 ± 0.7	0.7 ± 0.007	14.7 ± 0.9
N13	7.2 ± 0.5	1.1 ± 0.011	6.4 ± 0.4	N27	10.4 ± 0.7	0.7 ± 0.007	14.8 ± 0.9
N14	15.0 ± 1.1	1.2 ± 0.012	12.7 ± 1.0				

The experimental results of $\dot{Q}_{cooling}$, $\dot{W}$, and *EER* in RIEC-1 varied under different OA conditions. N2 and N21 were performed with the same T_{OA}, $\dot{V}_{OA}$, and R_{EA} values, but with different ω_{OA} values. An increase of 3.7 g·kg^{-1} in ω_{OA} reduced the *EER* value from 11.3 to 6.6. N8 and N18 were performed under the same values of ω_{OA}, $\dot{V}_{OA}$, and R_{EA}, but with different T_{OA} values. An increase of 14 °C in the T_{OA} increased the *EER* value from 6 to 12.6. N12 and N13 were performed under the same T_{OA}, ω_{OA}, and R_{EA} values, but with different $\dot{V}_{OA}$ values. The increase of 1568 m^3·h^{-1} in $\dot{V}_{OA}$ reduced the *EER* value by 5.9 between tests N12–N16, owing to the increase in electrical-energy consumption of the fan. N17 and N18 were performed under the same T_{OA}, ω_{OA}, and $\dot{V}_{OA}$ values, but with different R_{EA} values. An increase of 0.4 in R_{EA} reduced the *EER* value by 6.7 in tests N17–N18, because the value of $\dot{V}_{SA}$ was reduced when R_{EA} increased; therefore, $\dot{Q}_{cooling}$ was also reduced.

A summary of the influence of each input parameter on the *EER* value for RIEC-1 is shown in Fig. 7. The $\dot{V}_{OA}$ and R_{EA} values were set to the mean values of the DOE ranges to show the influence of outdoor conditions on the *EER*, as shown in Fig. 7a. The T_{OA} and ω_{OA} values were also set to the mean values of the DOE ranges to show the influence of airflow values on the *EER*, as shown in Fig. 7b. It can be observed that the *EER* value was higher when the T_{OA} value increased and the ω_{OA} value decreased (see Fig. 7a). Fig. 7b shows that the *EER* value increased when both the $\dot{V}_{OA}$ and R_{EA} values reduced.

Experimental data from the same manufacturers of the RIEC-2, RIEC-3, and RIEC-4 systems (see Table 13 in the Supplementary Material section) were used to obtain the respective $\dot{Q}_{cooling}$ and $\dot{W}$ empirical models. A set of nine test points was considered to compare the energy performance of the four RIEC systems. These points (S1–S9) were defined as a combination of three T_{OA} and ω_{OA} values (see Table 4). The respective nominal $\dot{V}_{SA}$ values of each RIEC system were considered at test points S1–S9. The *EER* values for the four RIEC systems under different OA conditions, T_{OA}, ω_{OA}, and nominal airflow rates are shown in Fig. 8. The trend of the *EER* values for the RIEC-2, RIEC-3, and RIEC-4 systems was similar to that of the *EER* values described above for RIEC-1, according to the variation in the T_{OA} and ω_{OA} values (see Fig. 8). It was observed that the experimental *EER* values for the RIEC-3 and RIEC-4 were the same for the nine points. The RIEC-3 and RIEC-4 systems exhibited the same energy behaviour because RIEC-4 was equal to the set of two RIEC-3 in parallel (see Table 2). This behaviour was because the SA temperature value was the same. However, as the supply airflow in RIEC-4 was double that in RIEC-3, the cooling capacity and power consumption doubled. The highest values of *EER* for these RIEC systems were reached at points S3, S6, and S9 when the T_{OA} value was maximised in the range of 43 °C. The maximum *EER* values were found when ω_{OA} was the lowest value in the studied range (8.9 g·kg^{-1}), as shown in Fig. 8.

3.2. Correlation of empirical models

Empirical models were developed to predict the $\dot{Q}_{cooling}$, $\dot{W}$, and *EER* values of RIEC-1 under various operating conditions. The DOE results were used to fit the models. The values of the regression coefficients for each input variable, coefficients of determination, R^2, standard deviations of the residuals, and mean absolute errors (MAE) of the $\dot{Q}_{cooling}$, $\dot{W}$, and *EER* models for RIEC-1 are listed in Table 9. High R^2 values for $\dot{Q}_{cooling}$, $\dot{W}$, and *EER* of 0.9991, 0.9997, and 0.9973, were obtained, respectively (see Table 9).

Empirical models of $\dot{Q}_{cooling}$ and $\dot{W}$ were also obtained for RIEC-2, RIEC-3, and RIEC-4 (see Table 10). These linear-regression models showed slightly lower R^2 values than those of the RIEC-1 system, although they were in good agreement, with R^2 values greater than 0.95.

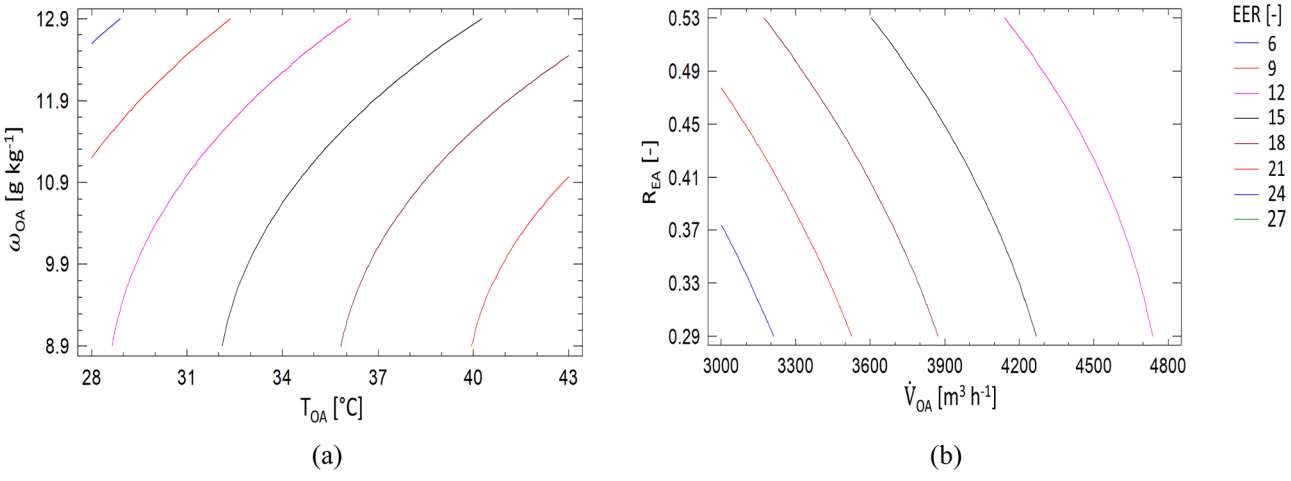

Fig. 7. Gradient plot of the *EER* for RIEC-1. Function of: (a) T_{OA} and ω_{OA}; (b) $\dot{V}_{OA}$ and R_{EA}.

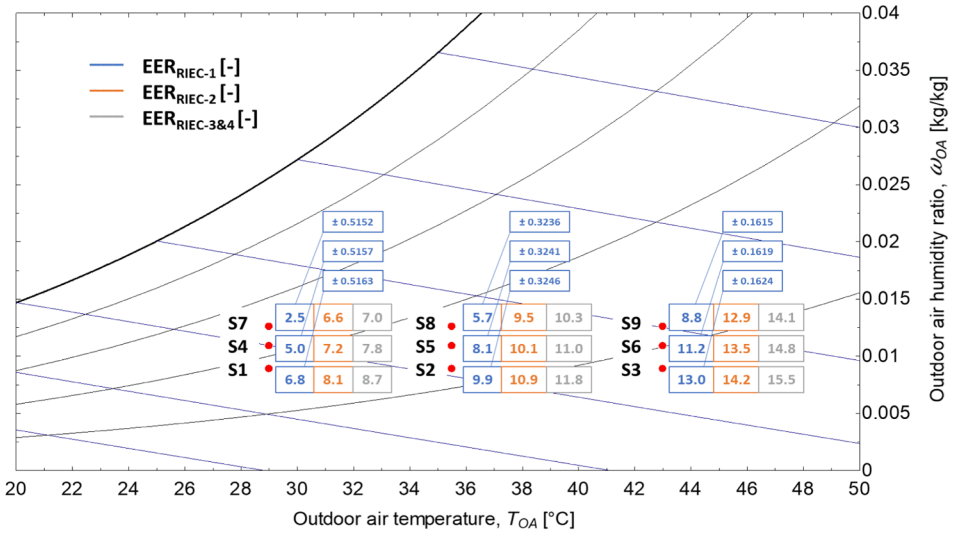

Fig. 8. EER values for the four RIEC systems according to the OA conditions.

Table 9
Estimated parameters and statistical indices of the RIEC-1 empirical models.

Estimated Parameters	Estimated Output value			Input Variables
	$\dot{Q}_{cooling}$	$\dot{W}$	*EER*	
b_0	−69468.500	−576.091	−12.288	–
b_1	834.281	2.450	2.942	T_{OA}
b_2	5079.290	10.601	3.533	ω_{OA}
b_3	13.204	0.046	−0.015	$\dot{V}_{OA}$
b_4	39435.300	907.679	−8.761	R_{EA}
b_5	−7.040	−0.034	−0.009	T_{OA}^2
b_6	−213.368	−0.491	−0.297	ω_{OA}^2
b_7	−0.001	6.413E-05	1.376E-06	$\dot{V}_{OA}^2$
b_8	−18754.300	−655.992	−16.675	R_{EA}^2
b_9	3.438	–	–	$T_{OA} \cdot \omega_{OA}$
b_{10}	0.132	–	−2.870E-04	$T_{OA} \cdot \dot{V}_{OA}$
b_{11}	−756.924	–	−1.055	$T_{OA} \cdot R_{EA}$
b_{12}	−0.507	–	3.580E-04	$\omega_{OA} \cdot \dot{V}_{OA}$
b_{13}	433.399	–	–	$\omega_{OA} \cdot R_{EA}$
b_{14}	−3.965	−0.084	0.011	$\dot{V}_{OA} \cdot R_{EA}$
R^2 [-]	0.9991	0.9997	0.9973	
Std. dev. [-]	0.374	1.031	0.112	
MAE [-]	81.720	3.325	0.265	

3.3. Results of SEER

3.3.1. Simplified calculation method

The annual performances of the four RIEC systems were evaluated using the proposed simplified calculation method and the $SEER_{simplified}$ values were calculated using Eq. (6). The number of hours of each partial load and climate zone was obtained to perform the simplified SEER calculation method using the temperature ranges listed in Table 6. Fig. 9 shows the H_A, H_B, H_C, and H_D values for each selected city.

The five climate zones with the longest (5850.2 h) to shortest (2740.0 h) cooling periods were Cairo, Murcia, Napoli, Pescara, and Madrid in order. Different values of H_A, H_B, H_C, and H_D were obtained for the climate zones owing to different climate severities, as shown in Fig. 9. The cities from the highest H_A value (242.0 h) to the lowest H_A value (3.5 h) were Cairo, Madrid, Pescara, Napoli, and Murcia in turn.

The results of $\dot{Q}_{cooling}$ and $\dot{W}$ for each experimental test (A, B, C, and D) in each RIEC were obtained using empirical models of the RIEC systems. Table 6 shows the values of the OA conditions and percentage of $\dot{V}_{SA}$ considered in the respective adjusted models. The ω_{OA} values considered in the four experimental tests were 11.5 g·kg^{-1} and Fig. 10 shows the contributions of each term described in Eq. (6). The results of the product of $\dot{Q}_{cooling}$ and $\dot{W}$ by PLF and H for each RIEC system and partial load in the five selected climates are shown in Fig. 10.

It was observed that the distribution of the values of $Q_{cooling}$ and W for all RIEC systems were similar, see Fig. 10. These values were also used to calculate the $SEER_{simplified}$ results according to Eq. (6), for each RIEC system in each climate zone (see Table 11), where each RIEC system showed similar $SEER_{simplified}$ values in all climate zones. The four RIEC systems showed the highest values of $SEER_{simplified}$ for Cairo and Madrid; that is, the climate zones with the highest H_A values. However, the RIEC systems showed the lowest value of $SEER_{simplified}$ for Murcia weather conditions, the city with the lowest climate severity in terms of T_{OA}; that is, with the lowest values of H_A and H_B during its cooling period. The $SEER_{simplified}$ results for RIEC-3 and RIEC-4 were the same because the RIEC-4 system was equal to the set of two RIEC-3 systems in parallel, as shown in Table 2. Similar $SEER_{simplified}$ values were obtained for each RIEC for the Murcia, Pescara, and Napoli weather conditions. These

Table 10
Estimated parameters and statistical indices of the RIEC-2, RIEC-3, and RIEC-4 models.

Estimated Parameters	Estimated Output value						Input Variables
	RIEC-2		RIEC-3		RIEC-4		
	$\dot{W}$	$\dot{Q}_{cooling}$	$\dot{W}$	$\dot{Q}_{cooling}$	$\dot{W}$	$\dot{Q}_{cooling}$	
b_0	−1074.00	−15533.27	−2491.00	−91061.53	−4982.00	−182123.06	–
b_1	−4.65E^{-14}	1108.59	−5.19E^{-14}	6372.59	−1.04E^{-13}	12745.18	T_{OA}
b_2	1.99E^{-13}	−990.05	−2.43E^{-13}	−5647.43	−4.87E^{-13}	−11294.86	$T_{OA,wb}$
b_3	0.74	4.17	0.52	4.04	0.52	4.04	$\dot{V}_{SA}$
R^2 [-]	0.9670	0.9612	0.9683	0.9515	0.9683	0.9515	
Std. dev. [-]	1.215	19.101	5.842	128.253	11.682	256.567	
MAE [-]	200.282	1013.692	351.582	6763.316	703.165	13526.633	

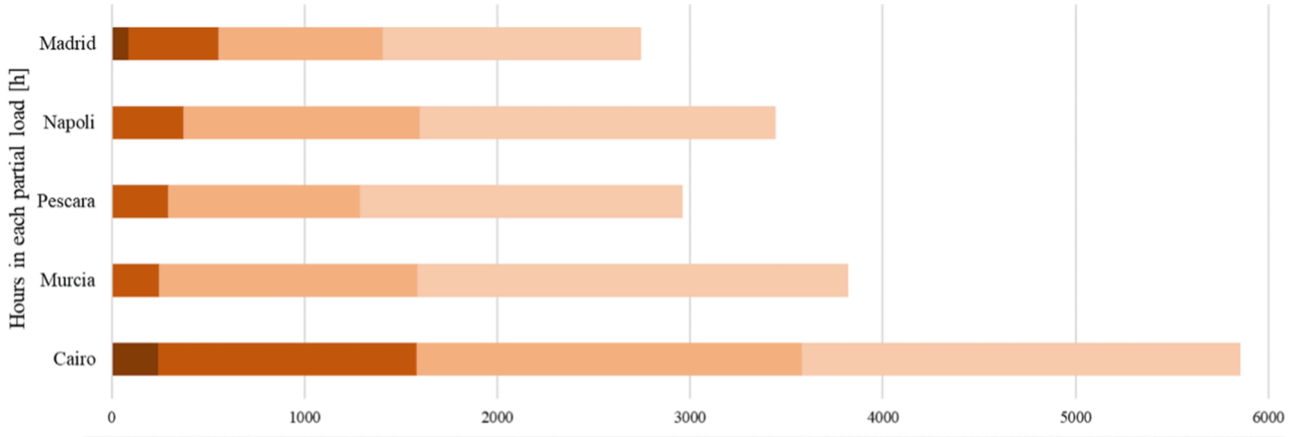

	Cairo	Murcia	Pescara	Napoli	Madrid
$T_{OA,avg}$ [°C]	25.0	22.6	22.9	23.1	24.0
H_A [h]	242.0	3.5	8.5	5.3	87.3
H_B [h]	1341.0	242.1	285.9	369.4	468.0
H_C [h]	1999.3	1341.3	996.8	1224.2	852.4
H_D [h]	2267.9	2230.3	1663.8	1842.1	1332.4

Fig. 9. Distribution of the number of hours for each partial load and climate zone.

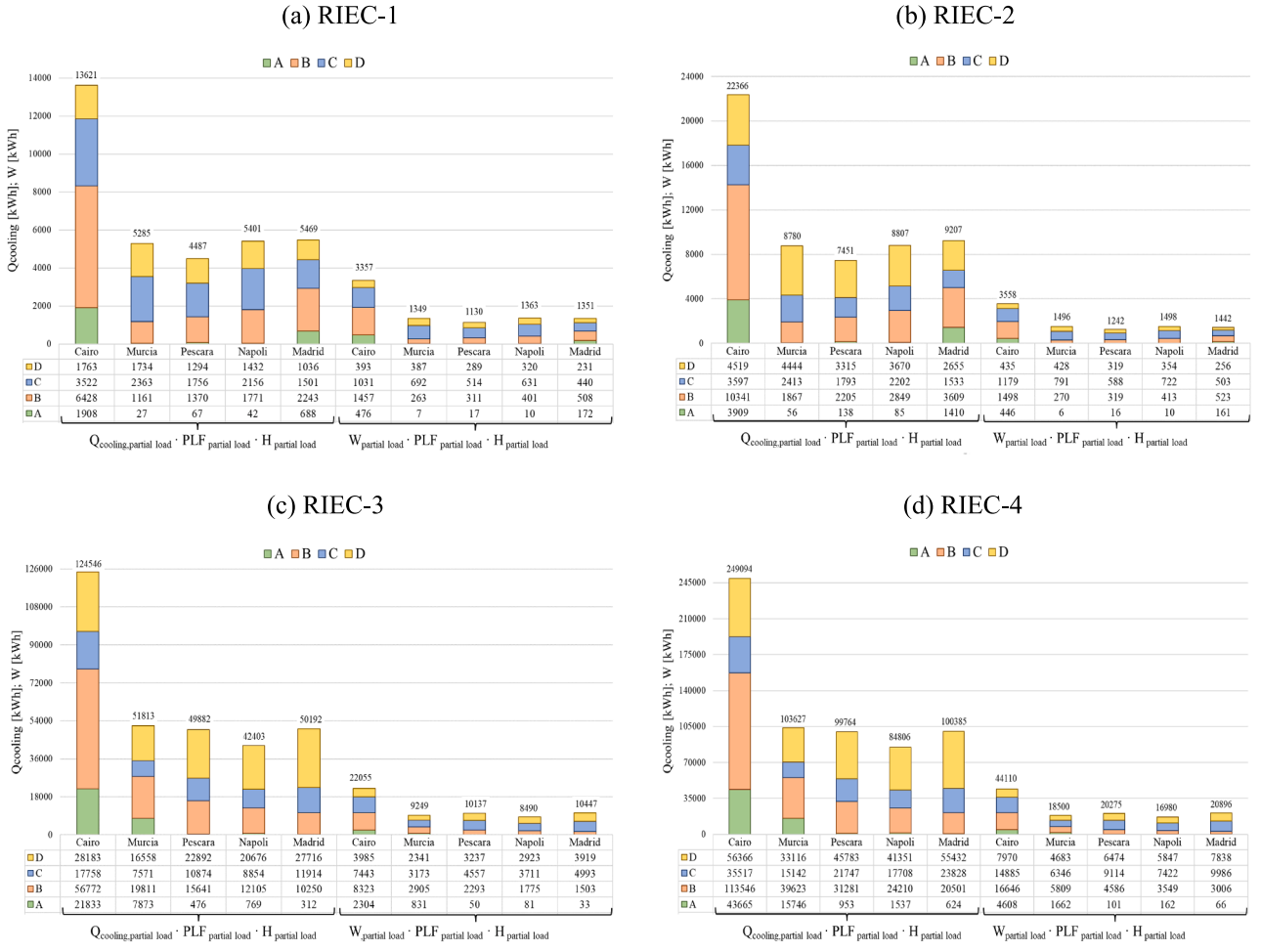

Fig. 10. Distribution of cooling capacity and energy consumption according to RIEC working at partial loads (experimental test points A, B, C, and D).

cities showed similar low climate severity in terms of $T_{OA,avg}$, with average values of approximately 23 °C (see Table 7). The main finding was that the $SEER_{simplified}$ value increased when the H_A value increased. The *EER* value also increased when the T_{OA} value increased, according to the *EER* empirical model of the RIEC systems (see Fig. 8).

Table 11
SEER results based on the simplified calculation method.

Climate zone	$SEER_{simplified}$ RIEC-1 [-]	$SEER_{simplified}$ RIEC-2 [-]	$SEER_{simplified}$ RIEC-3&4 [-]
Cairo	4.1	6.3	5.7
Murcia	3.9	5.9	4.8
Pescara	4.0	6.0	5.0
Napoli	4.0	5.9	4.9
Madrid	4.1	6.4	5.6

3.3.2. Detailed calculation method

Regression models of $\dot{Q}_{cooling}$ and $\dot{W}$ were integrated into the TRNSYS tool. Detailed energy simulations were performed to calculate the $SEER_{detailed}$ values for each RIEC system and the five selected climate zones in the Mediterranean region. The results of the annual cooling capacity and electrical-energy consumption for RIEC-1, RIEC-2, RIEC-3, and RIEC-4 in each selected climate zone are shown in Fig. 11. The climate zones with the highest annual cooling capacity and electrical-energy consumption were Cairo, Murcia, Napoli, Pescara, and Madrid; that is, the cities with the highest number of hours in the cooling period. The number of hours of each cooling period listed in Table 7 is directly related to the SEER results. Despite the longer cooling period of Pescara than that of Madrid, all RIEC systems showed increased values of total $\dot{Q}_{cooling}$ and total $\dot{W}$ for Madrid weather conditions (see Fig. 11). This was because the average T_{OA} value was higher in Madrid than that of Pescara, and the average ω_{OA} value was lower in Madrid than that of Pescara (see Table 7).

Based on these results, the $SEER_{detailed}$ expression in Eq. (7) obtained its values for all combinations of the RIEC systems and the representative cities of the Mediterranean climate region (see Table 12). The values of $SEER_{detailed}$ for the RIEC-3 and RIEC-4 systems were the same values for all cities because the RIEC-4 system was equal to the set of two RIEC-3 systems in parallel (see the technical characteristics indicated in Table 2). Each RIEC system showed similar $SEER_{detailed}$ values for all climate zones. The highest values of $SEER_{detailed}$ for the four RIEC systems were obtained for the weather conditions of Cairo, Murcia, and Madrid (see Table 12). The average ω_{OA} value in these three cities was the minimum value of the range shown in Table 7, which was approximately 10 g·kg^{-1} during the respective cooling periods. However, the climate zones of Pescara and Napoli showed maximum average ω_{OA} values in the range of approximately 12 g·kg^{-1} and minimum average T_{OA} values in the range of approximately 23 °C (see Table 7). These two cities showed the lowest $SEER_{detailed}$ values for all RIEC systems (see Table 12). Therefore, the behaviours of the *EER* and *SEER* with respect to the OA conditions, T_{OA} and ω_{OA}, were similar.

A comparative analysis of both the SEER calculation methods was performed. The $SEER_{simplified}$ and $SEER_{detailed}$ results were used to obtain the *RE* according to Eq. (8). The *RE* values and the average relative error

Table 12
SEER results based on the detailed calculation method.

Climate zone	$SEER_{detailed}$ RIEC-1 [-]	$SEER_{detailed}$ RIEC-2 [-]	$SEER_{detailed}$ RIEC-3&4 [-]
Cairo	4.0	6.3	5.8
Murcia	4.3	6.4	5.3
Pescara	3.9	5.5	4.7
Napoli	4.1	6.1	5.1
Madrid	4.3	6.2	5.5

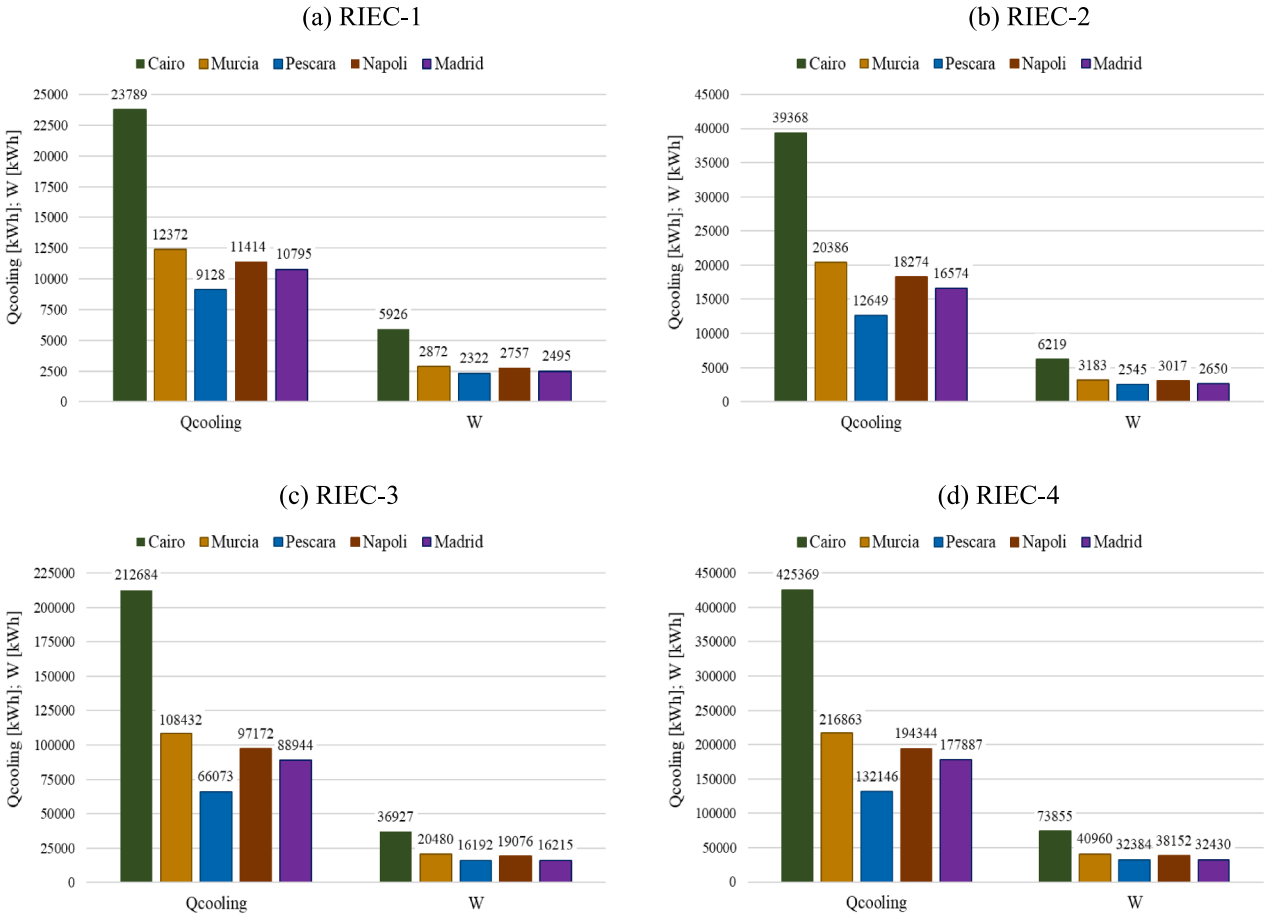

Fig. 11. Annual cooling capacity and electrical-energy consumption in each city.

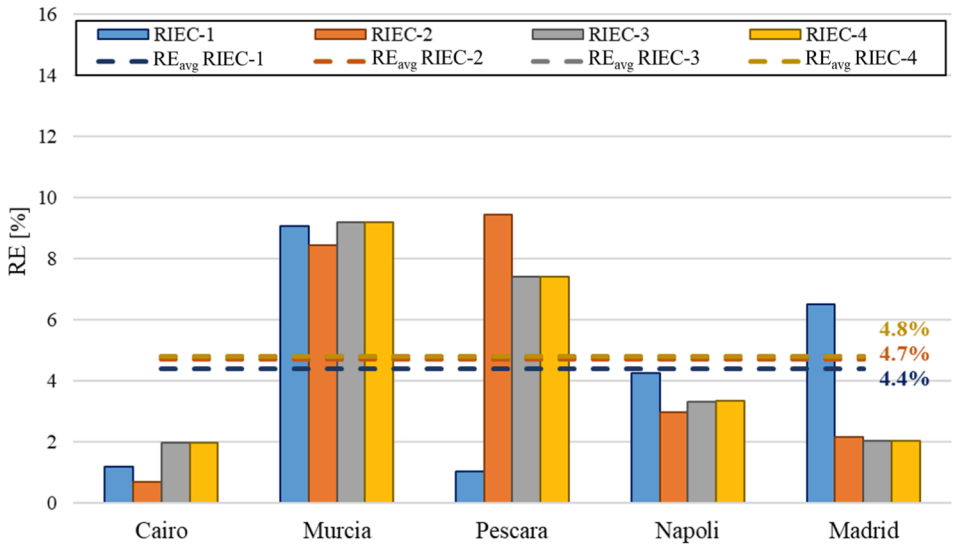

Fig. 12. RE between $SEER_{detailed}$ and $SEER_{simplified}$ values.

(RE_{avg}) for all RIEC systems and climate zones are shown in Fig. 12.

Cairo and Madrid climate zones showed the lowest *RE* values, being the cities with the highest climate severity according to T_{OA}. However, the RIEC systems for the weather conditions of Murcia and Pescara exhibited the highest *RE* values because of the higher values of oscillation in ω_{OA}. Napoli showed an *RE* value below 4.5% for all the RIEC systems. The global RE_{avg} value between the detailed and simplified SEER calculation methods for the RIEC systems in the Mediterranean climate region was 4.6%.

4. Limitations of this study

The technical aspects of the four RIEC systems investigated in this study were composed of an efficient counterflow heat exchanger whose PVC film with hydrophilic material and channel sizes were the same for all RIEC systems; only the number of heat exchanger cores varied. The ranges of nominal airflow and cooling capacity of the analysed RIEC systems were wide: 2880–46080 $m^3 \cdot h^{-1}$ and 18–118 kW. Based on the weather conditions, five cities were selected to represent the climate zones of the Mediterranean area because of their severe climatic conditions, particularly during the summer season. For other configurations of IEC, air flows, cooling capacities, climate conditions, and cooling capacity control strategies, the SEER results obtained using the simplified method proposed herein may not be valid.

5. Conclusions

In this study, a new testing and calculation method for the SEER of RIEC was developed. The experimental data of four RIEC systems were collected to obtain several empirical models, namely cooling capacity, $\dot{Q}_{cooling}$, power consumption, $\dot{W}$, and EER. Different input parameters were considered in the DOE—T_{OA}, ω_{OA}, $\dot{V}_{OA}$, and R_{EA}. Two methods for calculating the SEER were compared for four regenerative IEC systems and five different climate zones in the Mediterranean region (Cairo, Murcia, Pescara, Napoli, and Madrid). The detailed SEER calculation method for RIEC simulated the annual energies using the TRNSYS software. An alternative simplified methodology was developed for calculating the SEER in RIEC. This method is based on a regenerative indirect evaporative cooler study at four specific test points (A, B, C, and D).

The following conclusions are drawn based on the findings of this study.

- The results indicated that the simplified SEER calculation method for RIEC systems in the Mediterranean climate region proposed in this study could be an effective method for calculating SEER without the need to use annual energy simulations or measurements. Four load factors (PLF_A, PLF_B, PLF_C, and PLF_D) were used to minimise the calculation error between the SEER calculation methodologies. The mean RE with respect to the detailed SEER calculation method based on annual energy simulations was 4.6%.
- The SEER had a strong influence on weather conditions. The highest $SEER_{detailed}$ values were achieved for the Cairo and Madrid weather conditions of 5.8 and 5.5, respectively. These cities showed the highest $T_{OA,avg}$ and lowest $\omega_{OA,avg}$ values of approximately 25 °C and 10 $g \cdot kg^{-1}$, respectively. The four RIEC systems also reached the highest values of $SEER_{simplified}$ for Cairo and Madrid of 5.7 and 5.6, respectively. These climate zones yielded the highest H_A values; that is, the highest number of hours in which the T_{OA} exceeded 33 °C.

The findings can guide future studies focusing on seasonal performance and sustainable environments. The proposed methodology for calculating the SEER for RIEC can be used to obtain the carbon footprint and perform life-cycle analysis.

Declaration of Competing Interest

The authors declare that they have no known competing financial interests or personal relationships that could have appeared to influence the work reported in this paper.

Data availability

Data will be made available on request.

Acknowledgments

The authors acknowledge the financial support received by European Union's Horizon 2020 research and innovation programme, through the research project WEDISTRICT, reference H2020-WIDESPREAD2018-03-857801, and the support received in the form of data by the manufacturer Seeley International, from the regenerative indirect evaporative cooler units analysed in this research work.

Appendix A. Supplementary data

Supplementary data to this article can be found online at https://doi.org/10.1016/j.applthermaleng.2022.119710.

References

[1] Z. Duan, et al., Indirect evaporative cooling: Past, present and future potentials, Renew. Sustain. Energy Rev. 16 (9) (Dec. 2012) 6823–6850.
[2] F. Comino, J. Castillo González, F.J. Navas-Martos, and M. Ruiz de Adana, Experimental energy performance assessment of a solar desiccant cooling system in Southern Europe climates, Appl. Therm. Eng., vol. 165, no. September 2019, p. 114579, 2020.
[3] F. Comino, M. Ruiz de Adana, F. Peci, Energy saving potential of a hybrid HVAC system with a desiccant wheel activated at low temperatures and an indirect evaporative cooler in handling air in buildings with high latent loads, Appl. Therm. Eng. 131 (2018) 412–427.
[4] S. Delfani, J. Esmaeelian, H. Pasdarshahri, M. Karami, Energy saving potential of an indirect evaporative cooler as a pre-cooling unit for mechanical cooling systems in Iran, Energy Build. 42 (11) (2010) 2169–2176.
[5] S.J. Oh, et al., Approaches to energy efficiency in air conditioning: A comparative study on purge configurations for indirect evaporative cooling, Energy 168 (2019) 505–515.
[6] D. Pandelidis, A. Cichoń, A. Pacak, S. Anisimov, P. Drąg, Counter-flow indirect evaporative cooler for heat recovery in the temperate climate, Energy 165 (2018) 877–894.
[7] H. Caliskan, A. Hepbasli, I. Dincer, V. Maisotsenko, Thermodynamic performance assessment of a novel air cooling cycle: Maisotsenko cycle, Int. J. Refrig. 34 (4) (2011) 980–990.
[8] A. Ahmad, S. Rehman, L.M. Al-Hadhrami, Performance evaluation of an indirect evaporative cooler under controlled environmental conditions, Energy Build. 62 (2013) 278–285.
[9] J. Lee, D.Y. Lee, Experimental study of a counter flow regenerative evaporative cooler with finned channels, Int. J. Heat Mass Transf. 65 (2013) 173–179.
[10] S. Kashyap, J. Sarkar, and A. Kumar, Comparative performance analysis of different novel regenerative evaporative cooling device topologies, Appl. Therm. Eng., vol. 176, no. August 2019, p. 115474, 2020.
[11] C. Guo, Q. Liu, B. Zheng, Y. You, and Y. Li, Development of model based on condensation area ratio and effect on heat transfer capacity of indirect evaporative cooling, Appl. Therm. Eng., vol. 164, no. May 2019, p. 114557, 2020.
[12] Q. Liu, C. Guo, X. Ma, Y. You, Y. Li, Experimental study on total heat transfer efficiency evaluation of an indirect evaporative cooler, Appl. Therm. Eng. vol. 174, no. January (2020), 115287.
[13] S. Pourahmad, S.M. Pesteei, H. Ravaeei, S. Khorasani, Experimental study of heat transfer and pressure drop analysis of the air/water two-phase flow in a double tube heat exchanger equipped with dual twisted tape turbulator: Simultaneous usage of active and passive methods, J. Energy Storage 44 (PB) (2021), 103408.
[14] B. Fikri, E. Sofia, N. Putra, Experimental analysis of a multistage direct-indirect evaporative cooler using a straight heat pipe, Appl. Therm. Eng. 171 (February) (2020), 115133.
[15] A. Sohani, H. Sayyaadi, N. Mohammadhosseini, Comparative study of the conventional types of heat and mass exchangers to achieve the best design of dew point evaporative coolers at diverse climatic conditions, Energy Convers. Manag. 158 (January) (2018) 327–345.
[16] F. Comino, M.J. Romero-Lara, M.R. de Adana, Experimental and numerical study of dew-point indirect evaporative coolers to optimize performance and design, Int. J. Refrig. (2022).
[17] D. C., R. Naik, S.C. Godi, C.K. Mangrulkar, and P. H.K., Thermal performance analysis of a mixed-flow indirect evaporative cooler, Appl. Therm. Eng., vol. 217, no. August, p. 119155, 2022.
[18] Y.G. Akhlaghi, X. Ma, X. Zhao, S. Shittu, J. Li, A statistical model for dew point air cooler based on the multiple polynomial regression approach, Energy 181 (2019) 868–881.
[19] D. Pandelidis, S. Anisimov, Application of a statistical design for analyzing basic performance characteristics of the cross-flow Maisotsenko cycle heat exchanger, Int. J. Heat Mass Transf. 95 (2016) 45–61.
[20] Z. Duan, C. Zhan, X. Zhao, X. Dong, Experimental study of a counter-flow regenerative evaporative cooler, Build. Environ. 104 (2016) 47–58.
[21] N.H. Kim, Performance of an indirect evaporative cooler (IEC) made of PET/cellulose composite sheet as wetting media, Appl. Therm. Eng., vol. 186, no. August 2020, p. 116492, 2021.
[22] H. Yang, W. Shi, Y. Chen, Y. Min, Research development of indirect evaporative cooling technology: An updated review, Renew. Sustain. Energy Rev. vol. 145, no. March (2021), 111082.
[23] Y. Wang, X. Huang, J. Chu, M. Qu, T. Li, and C. Dai, Analysis of polishing waste ceramic foam packing in evaporative cooling, Appl. Therm. Eng., vol. 212, no. November 2021, p. 118477, 2022.
[24] Y. Chen, X. Huang, T. Sun, J. Chu, Experimental study of plant fiber-polymer composite for indirect evaporative cooler application, Appl. Therm. Eng. 199 (September) (2021), 117543.
[25] V. Afonicevs, U. Strauts, N. Bogdanovs, A. Lesinskis, Evaporative cooling technology efficiency compared to traditional cooling system - Case study, Eng. Rural Dev. 19 (2020) 877–883.
[26] R. Tariq, N.A. Sheikh, A. Livas-García, J. Xamán, A. Bassam, V. Maisotsenko, Projecting global water footprints diminution of a dew-point cooling system: Sustainability approach assisted with energetic and economic assessment, Renew. Sustain. Energy Rev. 140 (May) (2020) 2021.
[27] W. Li, J. Wang, W. Shi, J. Lu, High-efficiency cooling solution for exhaust air heat pump: Modeling and experimental validation, Energy 254 (2022), 124396.
[28] Z. Duan, X. Zhao, J. Li, Design, fabrication and performance evaluation of a compact regenerative evaporative cooler: Towards low energy cooling for buildings, Energy 140 (2017) 506–519.
[29] R. Kousar, M. Ali, M.K. Amjad, and W. Ahmad, Energy, Exergy, Economic, Environmental (4Es) comparative performance evaluation of dewpoint evaporative cooler configurations, J. Build. Eng., vol. 45, no. October 2021, p. 103466, 2022.
[30] Y. Yang, C. Ren, C. Yang, M. Tu, B. Luo, J. Fu, Energy and exergy performance comparison of conventional, dew point and new external-cooling indirect evaporative coolers, Energy Convers. Manag. 230 (2021), 113824.
[31] M.J. Romero-Lara, F. Comino, M. Ruiz de Adana, Seasonal Analysis Comparison of Three Air-Cooling Systems in Terms of Thermal Comfort, Air Quality and Energy Consumption for School Buildings in Mediterranean Climates, Energies 14 (15) (Jul. 2021) 4436.
[32] A.F. Santos, P.D. Gaspar, and H.J.L. Souza, Measuring the energy efficiency of evaporative systems through a new index—evacop, Energies, vol. 14, no. 9, 2021.
[33] M. Lata, N. Purohit, and D. K. Gupta, Techno-economic assessment of trans-critical CO2 booster system with modified evaporative cooling for supermarket application in Indian context, Environ. Prog. Sustain. Energy, vol. 40, no. 2, 2021.
[34] K. Yang, et al., An integrated system of water-cooled VRF and indirect evaporative chiller and its energy saving potential, Appl. Therm. Eng. vol. 194, no. May (2021), 117063.
[35] E. C. Certification, Certification Manual of the Eurovent Certified Performance Mark, no. January.
[36] Ctn, 100 Climatización, "UNE-EN 14825:2019 Acondicionadores de aire, enfriadoras de líquido y bombas de calor con compresor accionado eléctricamente para la calefacción y la refrigeración de locales. EnsaYos Y Clasificación En Condiciones De Carga Parcial Y Cálculo Del REndimiEnt", 2019.
[37] Carrier, "Impacto de la Directiva Europea de EcoDiseño en las Bombas de Calor y Enfriadoras.".
[38] A.G. Devecioğlu, Seasonal performance assessment of refrigerants with low GWP as substitutes for R410A in heat pump air conditioning devices, Appl. Therm. Eng. 125 (2017) 401–411.
[39] S.H. Lee, Y. Jeon, B. Kim, S. Yun, Y. Kim, Simulation-based comparative seasonal performance evaluation of single-stage heat pump and modulated two-stage injection heat pump using rotary compressors with various cylinder volume ratios, Appl. Therm. Eng. 159 (December) (2019).
[40] S.H. Lee, Y. Jeon, H.J. Chung, W. Cho, Y. Kim, Simulation-based optimization of heating and cooling seasonal performances of an air-to-air heat pump considering operating and design parameters using genetic algorithm, Appl. Therm. Eng. 144 (May) (2018) 362–370.
[41] A.Y.T. Al-Zubaydi and G. Hong, Experimental study of a novel water-spraying configuration in indirect evaporative cooling, Appl. Therm. Eng., vol. 151, no. November 2018, pp. 283–293, 2019.
[42] F. Fakhrabadi, F. Kowsary, Optimal design of a regenerative heat and mass exchanger for indirect evaporative cooling, Appl. Therm. Eng. 102 (2016) 1384–1394.
[43] R. Tariq, N.A. Sheikh, J. Xamán, and A. Bassam, Recovering waste energy in an indirect evaporative cooler – A case for combined space air conditioning for human occupants and produce commodities, Build. Environ., vol. 152, no. November 2018, pp. 105–121, 2019.
[44] European Commission. Delegated Regulation (EU) 2022/759 of the Commission, which modifies Annex VII of Directive (EU) 2018/2001 of the European Parliament and of the Council with respect to a methodology for calculating the amount of renewable energy used for cooling and urban cooling systems, 14th December 2021.
[45] International Organization for Standardization. EN ISO 16890-1:2016: Air filters for general ventilation. Part 1: Technical specifications, requirements and classification system based upon particulate matter efficiency, ePM). https://www.iso.org/standard/57864.html.
[46] CEN. 2017. European Standard EN 16798-3:2017. "Energy performance of buildings - Ventilation for buildings - Part 3: For non-residential buildings – Performance requirements for ventilation and room-conditioning systems (Modules M5-1, M5-4). Brussels.
[47] "Seeley International. Climate Wizard." [Online]. Available: https://www.seeleyinternational.com/eu/commercial/brands/climate-wizard-emea/.
[48] Weather Data, Trnsys 17, vol. 8. Available online: http://www.trnsys.com/ (Accessed on 10 January 2022).
[49] S.A. Klein, TRNSYS 17: A Transient System Simulation Program, University of Wisconsin, Madison USA, SEL, 2006.
[50] M. Kottek, J. Grieser, C. Beck, B. Rudolf, F. Rubel, World map of the Köppen-Geiger climate classification updated, Meteorol. Zeitschrift 15 (3) (2006) 259–263.
[51] Joint Committee for Guides in Metrology (JCGM): Evaluation of measurement data – Guide to the expression of uncertainty in measurement, JCGM 100:2008(E) – in English Evaluation of measurement data, Pavillon de Breteuil, F-92312 Sèvres CEDEX, 1st edn., https://www.bipm.org/en/publications/guides.